Research article

Journal of RAMAN SPECTROSCOPY

Received: 4 April 2015 Revised: 7 May 2015 Accepted: 13 May 2015 Published online in Wiley Online Library: 15 July 2015

(wileyonlinelibrary.com) DOI 10.1002/jrs.4734

Silver-capped silicon nanopillar platforms for adsorption studies of folic acid using surface enhanced Raman spectroscopy and density functional theory

John J. Castillo,[a,b]* Tomas Rindzevicius,[a] Kaiyu Wu,[a] Ciro E. Rozo,[c] Michael S. Schmidt[a] and Anja Boisen[a]

The study of the interactions of folic acid (FA) with surface enhanced Raman scattering substrates is relevant for understanding its adsorption mechanism and for fabricating analytical devices for detection of malignant cells over-expressing folate receptors. This paper presents a study of the adsorption of FA on silver-capped silicon nanopillar substrates employing surface enhanced Raman scattering spectroscopy and density functional theory calculations. The experimentally observed vibrations from free FA and FA bound to the Ag surface display different vibrational spectra indicating chemical interaction of the molecule with the metal surface. Density functional theory calculations show that the Ag–FA interaction is primarily through the nitrogen from the pteridine ring anchoring to the Ag metal surface. To investigate the Ag–FA binding behavior further, the adsorption isotherm of FA on the silver-capped silicon nanopillar surface is estimated. The results show a positive cooperative Ag–FA binding mechanism. That is, adsorbed FA increases the affinity of new incoming FA molecules. Copyright © 2015 John Wiley & Sons, Ltd.

Additional supporting information may be found in the online version of this article at the publisher's web site.

Keywords: SERS; nanopillar; silver; folic acid; adsorption isotherm

Introduction

Among the various spectroscopic techniques, surface enhanced Raman scattering (SERS) has been widely used to elucidate information about the adsorption behavior of biomolecules on metal surfaces.[1,2] Furthermore, the fluorescence background displayed for some biomolecules is reduced when they are adsorbed on metal surfaces, and thus, the technique is useful in the study of biological samples.[3]

Recent developments in the synthesis and fabrication of new colloid metal nanoparticles and solid support-based SERS substrates have led to the detection at trace levels of different compounds.[4] SERS substrates can be divided into two groups, (1) colloid metal nanoparticles[5] and (2) roughened metallic surfaces.[6] The main limitation in using colloid metal nanoparticles is the tendency for nanoparticle conglomeration after the addition of the analyte, which often leads to poor reproducibility of the SERS spectra.[7] An ideal SERS substrate must have sufficient Raman signal enhancement to be able to detect the analyte while at the same time having a homogenous surface able to produce reproducible Raman spectra.[8]

Recently, we have developed a simple method to produce flexible, freestanding silver-capped nanopillar (Ag NP) structures suitable for SERS applications.[9,10] These Ag NPs produce a remarkably large enhancement of the Raman scattering signal. Yang *et al.*[11] utilized similar gold nanopillars as a probe in a bioassay for specific detection of vasopressin molecules in the pM regime. Surface homogeneity and reproducibility of the SERS signal enable Au and Ag NPs to be used as a reliable SERS platform for studies of the adsorption behavior of different biomolecules. Another prominent example is SERS substrates based on ordered arrays of Au nanofingers that display very high (~10^{10}) enhancement factors and relatively low (<10%) variations of the SERS intensity over an area of ~6.4 cm^2.[12–14]

Several research groups have studied the adsorption mechanisms of molecules on SERS active substrates employing both theoretical calculations and Raman scattering experiments. Qi *et al.*[15,16] combined SERS spectroscopy and density functional theory (DFT) calculations for studying adsorption of aniline on a silver mirror surface. Pagliai *et al.*[17] have reported a SERS study combined with X-ray photoelectron spectroscopy and DFT to investigate the orientation of adenine adsorbed on silver and gold surfaces. In the study of Zhang *et al.*,[18] the authors evaluated the adsorption behavior of nicotinic acid on a gold nanowire array using SERS and DFT calculations. The adsorption of biomolecules on SERS substrates increases the Raman scattering intensity by

* *Correspondence to: John Castillo, Grupo de Investigación en Bioquímica y Microbiología GIBIM, Universidad Industrial de Santander, Bucaramanga, Colombia. E-mail: jcasleon@uis.edu.co*

a *Department of Micro- and Nanotechnology, Technical University of Denmark, Lyngby 2800, Denmark*

b *Grupo de Investigación en Bioquímica y Microbiología GIBIM, Universidad Industrial de Santander, Bucaramanga, Colombia*

c *Grupo de Investigaciones Ambientales para el Desarrollo Sostenible, Facultad de Química Ambiental, Universidad Santo Tomas, Floridablanca, Colombia*

several orders of magnitude, which is important for vibrational studies, analysis, identification and quantification of the target compounds.[1,19,20] Jing *et al.*[21] studied the adsorption of L-cysteine because of its strong tendency to be adsorbed onto the surfaces of a variety of metals. SERS of adenine-containing micro-RNA chains has been obtained by adsorption on a new silver grass-like nanostructure.[22]

Folic acid (FA) is an essential nutrient and is one of the most studied biomolecules due to its role in biosynthetic processes, cell growth and DNA synthesis.[23] FA is known as vitamin B and is formed by a pteridine ring (pt), *p*-aminobenzoic acid (paba) and glutamic acid (GA) (see the inset in Fig. 1). Detection of FA and its analogues is critical to medical diagnosis.[24] Deficiency of FA and folate analogues can induce irreversible neurological damage in newborn infants.[25] Recently, there has been a considerable rise in the use of FA for the development of drug delivery systems[26] and probes for detection of cancer cells over-expressing folate receptors.[27] Several SERS studies have been carried out for sensing FA and cells over-expressing folate receptors. For example, Boca-Farcau[28] has used SERS-labeled silver nanotriangles for multimodal detection of human ovarian cancer cells. Silver nanoparticles created via ethylene-diaminetetraacetic were used for detection of FA in water and human serum. Hu *et al.*[29] developed a cancer diagnostic probe based on reduced graphene oxide and silver nanoparticles for detection of FA. A novel SERS binary substrate of graphene oxide was developed for ultrasensitive detection of FA.[30] Previous works have only focused on SERS studies for detecting FA, and there is little knowledge about the adsorption characteristics of FA on SERS active substrates such as nanoscale silver.

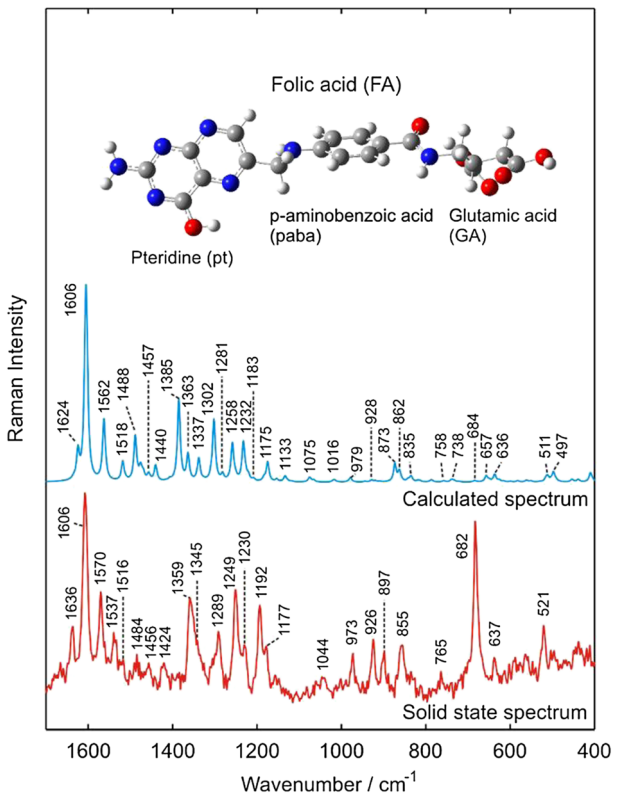

Figure 1. Density functional theory calculated (blue) and experimental (red) Raman spectra of solid-state folic acid. The inset shows the optimized geometry for folic acid.

In this study, we examine the adsorption of FA on silver metal nanostructures using SERS and *ab initio* calculations. In order to investigate the binding of FA to nanostructured Ag, SERS active Ag NP substrates were utilized. The DFT method was employed to obtain vibrational spectra of free FA and FA bound to a cluster of ten silver atoms (Ag10). We evaluate the binding properties of FA molecules on the surface of Ag NPs using different FA concentrations.

Experimental

Measurement tools and techniques

Raman scattering and SERS measurements were performed using a Thermo Scientific DXR Raman microscope. An optical microscope was coupled to a single grating spectrometer with 5-cm^{-1} full width at half maximum spectral resolution and ±0.5-cm^{-1} accuracy. A frequency-stabilized single diode laser was operated at 532 nm.

Raman scattering spectrum of FA was collected using a 10× long working distance objective, 20-mW laser power and 5-s signal accumulation times. FA SERS spectra were recorded using a 10× long working distance objective, 0.1-mW laser power and 5-s signal accumulation times. The power density was kept ~12 kW cm^{-2} at the sample to minimize photoinduced and thermal effects.[9]

In order to characterize the formation of FA layers adsorbed on Ag NPs, scanning electron microscopy (SEM) images were recorded using a Quanta FEG SEM microscope (Oregon, USA) with a maximal spatial resolution of 1.0 nm. Backscattered electrons were collected by an in-lens detector to gain contrast among areas with different chemical compositions. An acceleration voltage of 5.0 kV and a working distance of 2.6 nm was used. The angle between the incident electron beam and the surface of the Ag NP was 90° and 5° for top view and cross-sectional imaging, respectively.

Fabrication of SERS active Ag NP substrates

The substrates were fabricated, employing reactive ion etching of Si and silver metal deposition processes yielding vertical freestanding Ag NP structures surrounded by a continuous silver film at the base of the pillars.[9,10] The obtained Ag NP density is ~18 pillars μm^{-2}. Ag NP dimensions are the following: Ag NP height ~600 nm, Si pillar width ~50 nm and Ag cap height and width are ~300 and 120 nm, respectively. All fabricated Ag NP structures were stored in a desiccator and utilized within 3 days to minimize any effects related to oxidation of the Ag surface.

Preparation of FA solutions

Folic acid was obtained from Sigma-Aldrich Corp. All chemicals used in this study were of analytical grade. FA solutions were prepared as described by Castillo *et al.*[23] FA molecules were dissolved in water with an addition of 50 µl of NaOH (1 M) because of the poor solubility of FA. The FA powder (0.029 g) was mixed with H_2O (25 ml) until final pH 10 and magnetically stirred until a yellow-to-clear transition was observed.

FA isotherms

Serial dilutions of FA solutions in the range of 10^{-6} mol l^{-1} were prepared. Droplets (~1 µl) of various freshly prepared FA concentrations were then deposited on the SERS active substrates and left to dry. The droplets spread over the whole Ag NP surface area

Journal of RAMAN SPECTROSCOPY

($5 \times 5\ mm^2$) in several minutes to ensure homogeneity in the surface coverage and to achieve a suitable time of adsorption equilibrium and thus to avoid any change of desorption of FA. Before every SERS measurement, Ag NP-FA were gently rinsed with Milli-Q water and dried with nitrogen flow to remove the non-adsorbed FA. The Raman scattering signal was recorded over an area of ~0.05 mm^2 with 17 and 11 μm *x* and *y* step sizes, respectively.

Surface enhanced Raman scattering maps for each concentration were performed using an exposure time of 5 s/spectra was used, and 238 spectra were obtained. The averaged 681-cm^{-1} peak intensity from 238 spectra was used for the construction of the isotherm plot.

Computational methods

In order to identify the main vibrations of FA Raman scattering spectra, its vibrational frequencies were calculated using the DFT method with B3LYP theory combined with the standard 6-31G(d) basis set. The calculated frequencies were scaled by a factor of 0.9614 in accordance with the results reported in the study of Sakata *et al.*[31] with the purpose to correct for systematic errors. A cluster of Ag atoms were chosen as a model system for the Ag NP structures.[31] In a similar work,[12] a cluster composed of six or eight silver atoms was employed to simulate the adsorption of FA on metallic SERS substrates under the influence of the temperature. In order to decrease the high computational demands for larger clusters and to have a surface cluster with enough dimensions to interact with FA, a cluster of ten Ag atoms (Ag10) was selected and proven to be a good candidate for simulating the Ag–FA SERS spectrum. The Ag10 cluster was planar and large enough to cover a representative part of FA (see the inset in Figs. 2). The interaction between FA and Ag10, the Ag10–FA geometry optimization and the Raman spectra were computed using the scalar relativistic effective core potential with double-zeta basis sets (LANL2DZ).[32,33] All the geometries of the model system were fully optimized. In addition, the highest occupied molecular orbital–lowest unoccupied molecular orbital energy gap and the chemical hardness[34] of the FA molecule were also calculated, (Supporting Information; Fig. S1). The calculations were carried out using the GAUSSIAN 09 software package.[35]

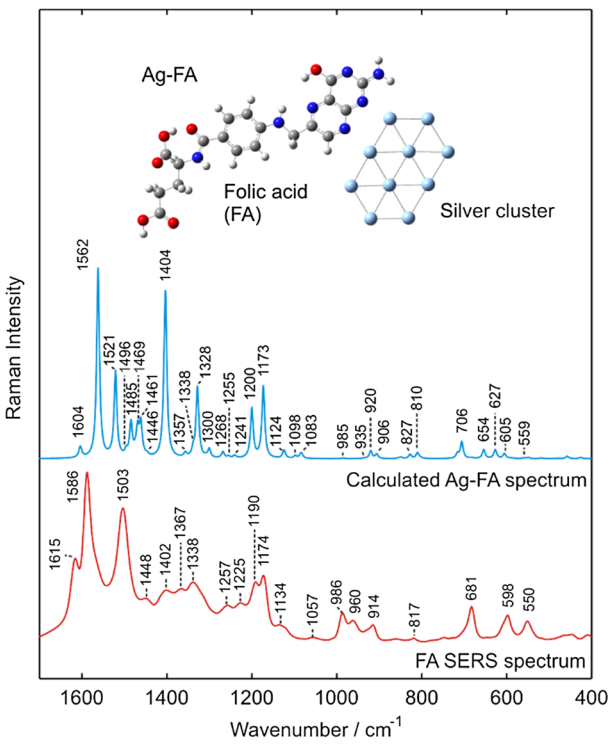

Figure 2. Density functional theory calculated (blue) and experimental (red) surface enhanced Raman scattering (SERS) spectra of folic acid using silver-capped silicon nanopillar substrates. The inset shows optimized geometry for folic acid adsorbed on a cluster of ten silver atoms.

Results and discussion

Raman spectra of FA

Even though the SERS spectra of FA have been investigated experimentally both on colloids and metallic surfaces,[12,19,20] to the best

Table 1. Assignment of experimental and calculated Raman modes of the FA molecule (solid state)

Raman	Calculated	Assignments
1636(m)	1635	ρ(OH)s(NH$_2$)ν(C=N)(pt)
	1624	ν(C=C)(C=O)ρ(NH)(paba)
1606(s)	1606	s(NH$_2$)ν(C=N)(pt); ν(C=C)ρ(CH)(paba)
1570(s)	1562	s(NH$_2$)ν(C=N)ρ(OH)(pt); ρ(NH)ν(C=C)(paba)
1537(m)		
1516(w)	1518	ν(C=N)pt; ν(C=C)ρ(CH)(paba); ν(CN)(GA)
1484(w)	1488	ρ(NH)s(CH$_2$)ν(C=C)(paba); ρ(NH)s(CN)(GA)
	1476	s(NH$_2$)(CH$_2$)ρ(CH)(pt); ρ(NH)(paba)
	1469	s(CH$_2$)(pt); ρ(NH)(CH)(paba); ρ(NH)(GA)
1456(w)	1457	ν(C=C)ρ(CH)(pt); ρ(NH)(CH)(paba)
1424(w)	1440	s(CH$_2$)ν(C=N)ρ(CH)(OH)(pt)
	1385	ρ(CH$_2$)(OH)ν(C=N)(pt)
1359(s)	1363	ν(C=N)ρ(CH)(OH)ω(CH$_2$)(pt)
1345(m)	1337	ρ(CH)ω(CH$_2$)(pt); ρ(CH)(OH)(GA)
1289(s)	1302	ρ(OH)(CH)(pt); ρ(CH)(paba); ρ(NH)(OH)(CH)ω(CH$_2$)(GA)
	1281	ρ(CH)t(CH$_2$)(GA)
1249(s)	1258	ρ(CH)(paba); ρ(NH)(OH)(CH)ω(CH$_2$)(GA)
1230(m)	1232	t(CH$_2$)(pt); ρ(CH)(paba); ρ(NH)(OH)(CH)ω(CH$_2$)(GA)
1192(s)	1183	ρ(OH)ν(C=C)t(CH$_2$)(pt); ρ(CH)(paba)
1177(m)	1175	t(CH$_2$)(pt); ρ(CH)(paba)
	1133	ρ(CH)(paba); ρ(OH)ω(CH$_2$)(GA)
1044(w)	1075	ρ(CH$_2$)ν(C–C)(GA)
	1016	ν(C=N)ρ(NH$_2$)(OH)(CH$_2$)(pt)
973(m)	979	ρ(CH$_2$)ρ(OH)(CH$_2$)(pt); ρ(NH)(CH)(paba)
926(m)	928	ρ(CH)(pt) oop;
897(m)	873	b(C=C)(paba); ρ(OH)(GA)
855(m)	862	b(C=C)(paba); ρ(OH)t(CH$_2$)ν(C–C)(GA)
	835	ν(C=N)ρ(NH$_2$)(CH$_2$)(pt); ρ(OH)ρ(CH$_2$)t(CH$_2$)(GA)
765(w)	758	ρ(CH$_2$)(GA)
	738	ν(C=C)ρ(CH)(paba) oop def; ρ(OH)(GA)
682(s)	684	ν(C=N)ρ(CH)(OH)(pt) oop def; ρ(CH)(NH)(paba)
	657	ν(C=N)ρ(OH)(pt) def; ρ(NH)(CH)(paba) def
637(w)	636	ν(C=N)(pt) def; paba def; ρ(CH$_2$)ρ(OH)(GA);
521(m)	511	ρ(NH$_2$)(pt) def; ρ(NH)(CH)(paba) oop def
	497	ρ(NH)(paba)

m, medium; s, strong; w, weak; ν, stretching; δ, bending; ρ, rocking; ω, wagging; s, scissoring; t, twisting; b, breathing; oop, out of plane; def, deformation of pteridine rings or *p*-aminobenzoic acid ring; pt, pteridine; paba, *p*-aminobenzoic acid; GA, glutamic acid.

of our knowledge, there are no previous reports of the adsorption studies and computed vibrational frequencies of FA in metallic surfaces nanostructured. The assignment of Raman bands of FA in a previously reported study was incomplete,[19,20] and a deeper analysis of all vibrational modes of FA is warranted. In the following paragraph, the complete assignment of the Raman bands of FA is presented using both experimental and theoretical spectra (see summarized data in Table 1).

As mentioned, the FA molecule is made up of three parts: pt, paba and GA. In Fig. 1, calculated and experimental Raman scattering spectra of FA are compared. The inset in Fig. 1 shows the optimized structure of the FA molecule. The geometry of the FA structure and the interatomic distances and bond angles was optimized and is in good concordance with previous studies.[36] The calculated spectra in Fig. 1 exhibit a set of intense bands that can also be observed experimentally (~1600–1100-cm^{-1} region). The most intense experimentally observed bands are N–H and C=N vibrations (sNH_2, νC=N at 1606 cm^{-1}) from the pt ring, vibration of the C=C bonds of the aromatic ring moiety from paba (νC=C 1570 cm^{-1}), vibration of pt (νC=N 1359 cm^{-1}) and a C–H mode vibration of GA (ρCH 1289 cm^{-1}). These calculated frequencies are in agreement with the experimental frequencies recorded and in good concordance with a previous report about detecting FA on hybrid graphene oxide/Ag nanoparticle SERS substrate.[30] A set of medium intensity frequencies located at 1636, 1345, 1230 and 1177 cm^{-1} are associated to ρOH, ρCH from the pt ring and C–H vibration from the paba moiety, respectively. An additional medium-intensity wavenumber due to the breathing mode of *p*-aminobenzoic ring is located at 897 cm^{-1}. A group of three weak bands at 1516, 1484 and 1044 cm^{-1} are assigned to the stretching of C=C and C–N from the paba moiety, the stretching of C=C from the pt ring and the stretching of C-C from GA. Another weak intensity band is observed at 765 cm^{-1} and is attributed to the vibration CH_2 from GA. Apart from these weak bands, experimental data in

Table 2. Assignment of experimental and calculated Raman modes of the FA molecule adsorbed on the Ag surface

SERS	Calculated	Assignments
1615(m)	1604	$s(NH_2)\nu$(C=N)(pt); ν(C=C)ρ(CH)(paba)
	1602	$s(NH_2)\nu$(C=N)(pt); ν(C=C)ρ(CH)(paba)
1586(s)	1562	ν(C=N)(pt)ρ(OH)(pt); ν(C=C)ρ(NH)(paba)
1503(s)	1521	$s(NH_2)\nu$(C=N)ρ(CH)$s(CH_2)$(pt)
	1496	$s(CH_2)$(pt); ν(C–N)(C=C)ρ(CH)(paba); ρ(NH)ν(C=O)(GA)
	1485	$s(NH_2)(CH_2)\nu$(C=N)ρ(CH)(pt)
	1475	ρ(CH)$s(CH_2)$(pt); ρ(NH)(CH)(paba); ρ(NH)(GA)
	1469	ρ(CH)ν(C=C)$s(CH_2)$(pt); ρ(NH)(CH)(paba); ρ(NH)ν(C=N)$s(CH_2)$(GA)
1448(w)	1461	ν(C=N)$s(CH_2)$(pt); ρ(NH)(CH)(paba)
	1446	$\omega(CH_2)$(pt); ρ(NH)(CH)(paba); ρ(NH)$s(CH_2)\nu$(C=N)(GA)
1402(w)	1404	ν(C=C)(C–C)(C=N)(C–O)ρ(CH)$(NH_2)\omega(CH_2)$ (pt); ρ(NH)(CH)(paba)
1367(w)	1357	ρ(CH)$\omega(CH_2)$(pt); ν(C=C)(paba); ρ(OH)(GA)
	1338	ρ(CH)$\omega(CH_2)$(pt); ν(C=C)(C–N)ρ(CH)(paba)
1338(m)	1328	$\rho(CH_2)\nu$(C=C)ν(C–N)ν(C=N)ρ(CH)$\omega(CH_2)$(pt); ρ(CH)(paba)
	1300	ρ(CH)(paba); $\omega(CH_2)\rho$(NH)(OH)(GA)
	1268	ρ(NH)(CH)(paba)
1257(w)	1255	ρ(NH)(CH)(OH)$t(CH_2)$(GA)
1225(w)	1241	ρ(CH)(OH)(pt) def
1190(s)	1200	$\rho(NH_2)$(OH)(CH)$\omega(CH_2)$(pt); ρ(CH)(paba)
1174(s)	1173	ρ(OH)$\omega(CH_2)$(pt) def; ρ(CH)(paba)
1134(w)	1124	ρ(CH)(paba)
	1098	$\rho(NH_2)$(CH)(pt); ν(C–N)ρ(CH)(paba)
1057(w)	1083	$\rho(NH_2)$(CH)(OH)(pt) def; ν(C–N)(paba) def; ν(C–C)(GA) def
986(m)	985	ρ(OH)(pt) def; ν(C=C)ρ(CH)(paba) def
960(m)	935	ρ(OH)(GA)
914(m)	920	$\rho(NH_2)$(OH)(pt) def
	906	ρ(CH)(CH_2)(pt) oop
	827	*b*(C=C)(paba); $t(CH_2)\rho(CH_2)\nu$(C–C)(GA)
817(w)	810	ν(C–N)(paba) def; δ(CNO)ρ(OH)(CH_2)(GA)
681(s)	706	ν(C=N)ρ(CH)(OH)(pt) oop def; ν(C–C)(pt) def; ν(C–C)(pt–paba); ρ(CH)(paba) oop
	654	$\rho(NH_2)$(pt) ip def; (paba) ip def; $\rho(CH_2)$(GA)
	627	(pt) ip def; (paba) ip def;
598(m)	605	$\rho(NH_2)$(pt) oop; ρ(OH)(pt) ip def; $\rho(CH_2)\delta$(COO)(GA)
550(m)	559	$t(NH_2)\rho$(CH)(OH)(pt) oop

w, weak; m, medium; s, strong; ν, stretching; δ, bending; ρ, rocking; ω, wagging; *s*, scissoring; *t*, twisting; *b*, breathing; oop, out of plane; ip, in plane; def, deformation of pteridine rings or *p*-aminobenzoic acid ring; pt, pteridine; paba, *p*-aminobenzoic acid; GA, glutamic acid.

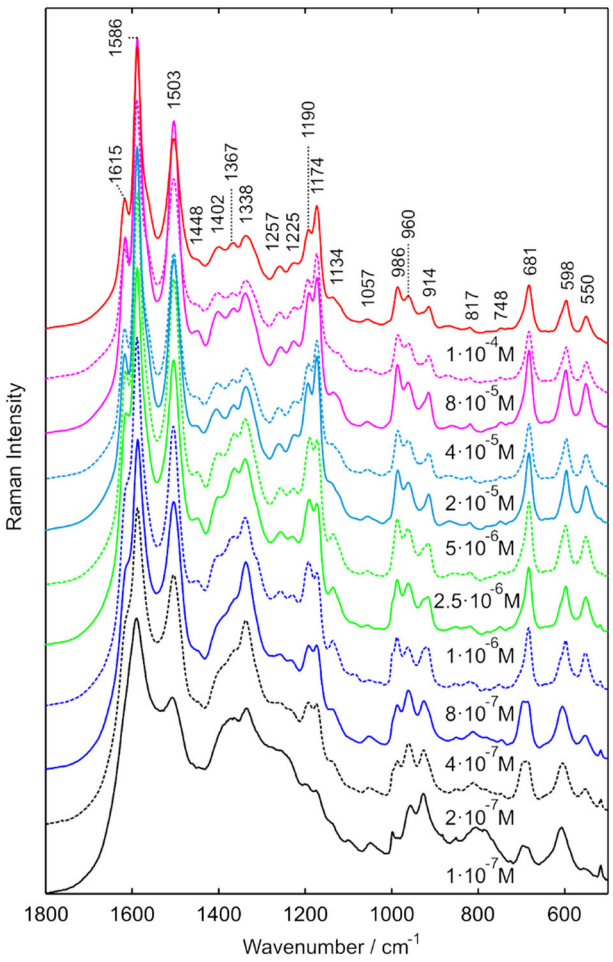

Figure 3. Surface enhanced Raman scattering spectra of different concentrations of folic acid adsorbed on silver-capped silicon nanopillar structures. All spectra were recorded for 5 s at a laser power of 0.1 mW using a 10× objective lens.

Journal of RAMAN SPECTROSCOPY

Fig. 1 show the presence of weaker modes found at 1044 and 637 cm^{-1}. The vibrations were assigned to the $\rho(CH_2)$ vibrational mode from the GA and a deformation of paba, respectively.

The calculated spectrum displays some deviations from the experimental results in the 1000–500-cm^{-1} region. A prominent example is a strong band found at 682 cm^{-1}. The calculated spectrum displays a weak mode at 684 cm^{-1}, which primarily derives from the stretch C–N and C–C of the pt ring and *p*-aminobenzoic fragment, respectively.

SERS spectra of FA

In connection to the FA Raman scattering results, we performed SERS measurements and DFT calculations to investigate the FA–Ag metal interaction. The presence of new bands and the relative intensification observed in SERS spectra compared with the normal Raman bands suggest an influence and close interaction of the atoms bound to the metal surface. The observed experimental spectra are described well using the Ag10 cluster-FA model system (Fig. 2 and Table 2). SERS spectra of FA are consistent with previous reported vibrational spectra obtained utilizing silver nanoparticle colloids.[30]

The most intense bands present in the FA Raman spectrum are also present in its SERS spectrum (Figs. 1, 2 and 3). Importantly, changes in both relative intensities and the positions of the vibrational modes are observed, indicating chemical interaction of the FA molecule with the Ag metal surface. In Fig. 3, the strongest SERS signals are located at 1586, 1503, 1174 and 681 cm^{-1}, which arise mainly from the stretching of C=C from paba, scissoring from NH_2 and deformation from the pt ring, respectively. The broad SERS peak at 1338 cm^{-1} from the stretching vibration of C=N(pt) is also an intense band, and it shows the strong interaction of nitrogen with silver. The interaction of nitrogen from the paba fragment with Ag NPs is further confirmed by the presence of the strong rocking vibration at 1174 cm^{-1}. In addition, nitrogen from NH_2 is in direct contact with the Ag surface as is shown by the vibration at 1586 cm^{-1}. The presence of the symmetric stretching mode of the C=N bond (681 cm^{-1}) in the SERS spectrum further supports the assumption that the FA is anchored to the Ag surface through a weak interaction with the benzene ring. The solid-state spectrum in Fig. 1 contains a set of weak bands at 1484, 1230 and 855 cm^{-1}, which are the vibrational modes from the symmetric stretching of CH, ρ(OH) and symmetric stretching of the bond O=N–C from the GA moiety, respectively. The absence of these bands in the FA SERS spectrum suggests that the GA fragment from FA is not involved in the interaction with the Ag surface. This indicates that only the pt ring is adsorbed on the surface of the Ag-coated silicon nanopillars.

Such changes in the FA SERS spectrum are corroborated by the calculated spectra obtained using the DFT method (Fig. 3). Our theoretical study suggests an adsorption model where the FA interacts with the Ag atoms primarily through the nitrogen atoms from the pt ring as shown in the inset in Fig. 3. In order to further verify the reliability of the aforementioned model, we have simulated three additional geometries placing the Ag10 cluster at different positions (Fig. 4) (model II, III and IV). The simulated SERS spectra from the model II show a weak interaction between the pt ring and the Ag10 cluster evidenced by the presence of weak vibrations from C–N belonging to the pt. A group of a set of bands at 1275, 1259 and 1241 cm^{-1} in the model II show that the main interaction with the cluster is with GA moiety. The simulated SERS spectra of model III show a weak interaction between the pt ring and the Ag10 cluster (1604 cm^{-1}), while the strongest vibrations come mainly from paba moiety and the cluster. On the other hand, the models I and II showed not only the most strong vibration coming from the nitrogen from pt ring and also the lowest values

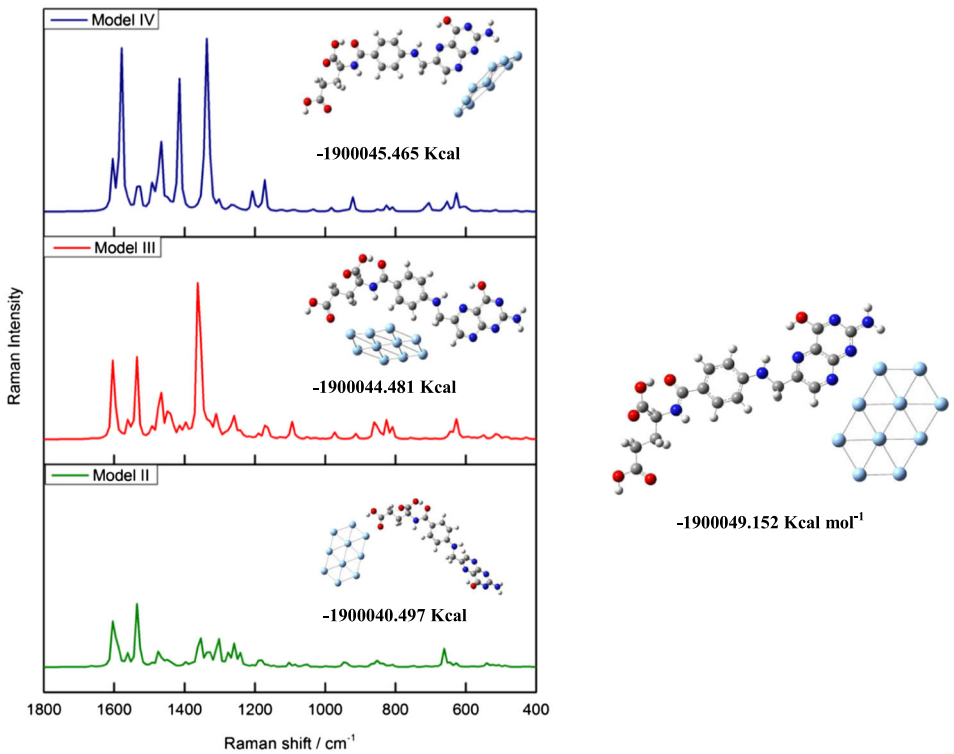

Figure 4. Different adsorption geometries and energy values of folic acid adsorbed on a cluster of ten silver atoms.

of energy, but the model I exhibited the lowest energy value ($\Delta E_{I-II} = -3.686939$ Kcal mol^{-1}), confirming thus that the most likely interaction with the Ag10 cluster is through the nitrogen of pt ring.

After performing the optimization, we find no reliable geometry alternatives as the obtained energy values are higher than the optimized geometry shown in model I of Fig. 4.

FA binding to the Ag surface and adsorption isotherm

The adsorption of FA on the Ag NP surface was studied further as a function of FA concentration. In Fig. 3 and 5, the SERS spectra of FA adsorbed on the Ag NP surface for 11 different FA solution concentrations between 1×10^{-7} and 1×10^{-4} M are presented. The results show that the FA spectral features are retained down to the nanomole regime. The maximum SERS intensity was observed at a concentration of 1×10^{-5} M.

The intensity of the SERS signal is related to the amount of FA adsorbed on the Ag NP surface. In Fig. 6, the concentration-dependent adsorption behavior of FA on Ag NPs is shown. Because FA binding to the Ag metal surface occurs via nitrogen atoms from the pt ring, the intensity of the symmetric stretching mode C=N at 681 cm^{-1} was selected as a marker peak (Fig. 3). The equilibrium SERS intensities of FA adsorbed on silver nanopillars were fitted by nonlinear curve analysis to the Hill equation[37] of the form

$$I_{SERS} = \frac{I_{max}\times FA^n}{K_{ads} + FA^n} \quad (1)$$

where I_{max} is the maximum recorded SERS intensity, FA is the concentration of FA solutions, K_{ads} is the equilibrium constant for dissociation and n is a cooperative constant.

When $n > 1$ or $n < 1$, attraction and repulsion between adsorbed molecules will take place, respectively. Note that when $n = 1$, the Hill equation behaves as the Langmuir isotherm. We obtained $K_{ads} = 2.4\times10^{-6}$M^{-1} and $n = 1.53$, which indicate that FA molecules that are already adsorbed to the Ag surface increase the affinity of

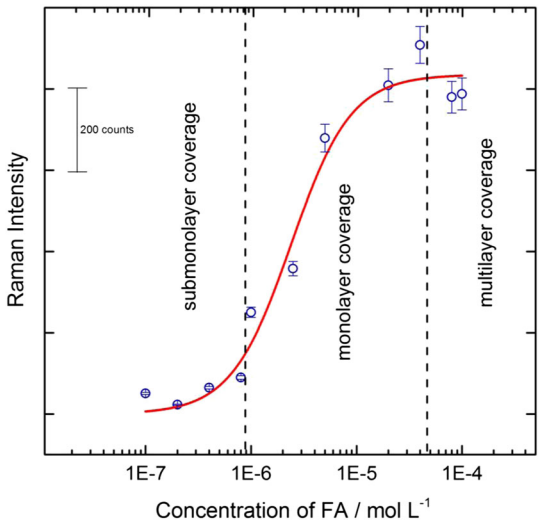

Figure 6. Summarized surface enhanced Raman scattering signal intensity changes for the different concentrations of folic acid (FA) adsorbed on silver-capped silicon nanopillar structures. The signal intensity is plotted for the 681-cm–1 mode. All spectra were recorded for 5 s at a laser power of 0.1 mW using a 10× objective lens.

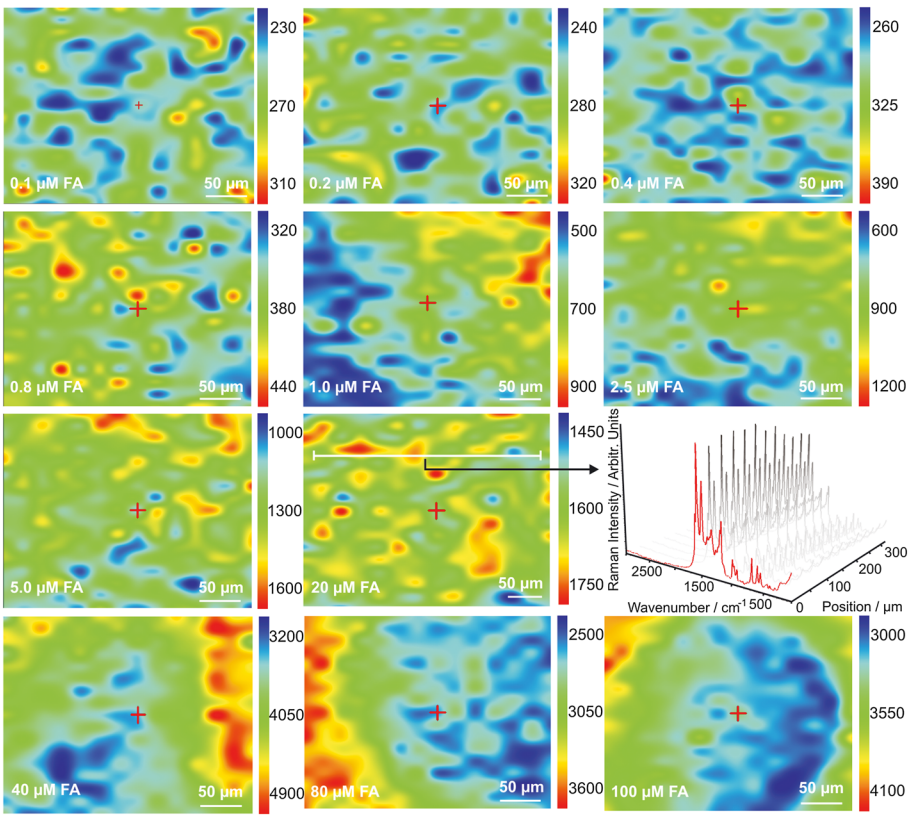

Figure 5. Surface enhanced Raman scattering (SERS) maps of the different concentrations of folic acid (FA). The maps show SERS intensity distribution of at 681 cm^{-1}. The SERS signal scanning area is 320 × 250 μm.

Journal of RAMAN SPECTROSCOPY

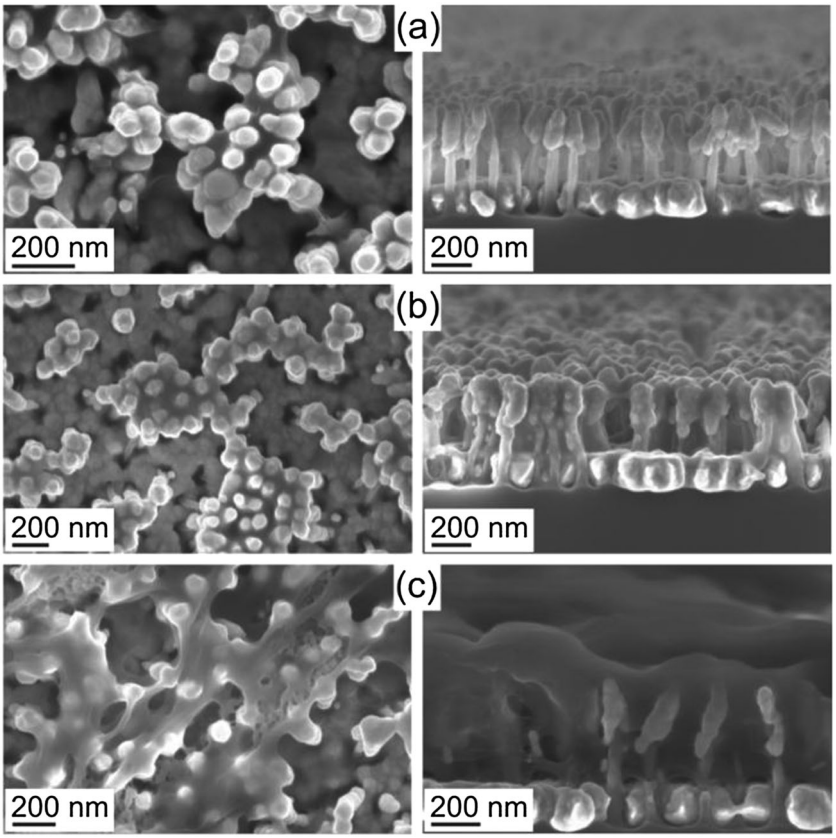

Figure 7. Scanning electron microscopy images of the top (left) and side view (right) of folic acid adsorbed on Ag-capped silicon nanopillar structures. (a) Submonolayer coverage at 2×10^{-7} M, (b) monolayer coverage at 1×10^{-6} M and (c) multilayer coverage at 2×10^{-5} M.

the new incoming FA molecules to the Ag metal surface. That is, the model shows a positive cooperative Ag–FA binding mechanism.

In the $\sim10^{-7}-10^{5}$-M region, the SERS signal intensities steadily increase because of an effective accumulation of FA molecules within the electromagnetic hot spots in the proximity of the Ag NPs where the Raman scattering signal is enhanced the most.[10] Thomas *et al.*[38] reported a similar behavior at low concentrations of carnosine adsorbed on silver nanoparticles. Likewise, higher concentrations of FA ($>10^{-5}$ M) leads to multilayer formations, and the observed SERS intensity is saturated. In addition, the measured SERS signals exhibit considerable intensity fluctuations (see the $>4\times10^{-5}$-M region in Fig. 6). To investigate this, the SERS substrates exposed to different FA concentrations were analyzed using SEM (Fig. 7). The SEM images reveal that an increased FA concentration ($>10^{-5}$ M) leads to inhomogeneous leaning of Ag NPs [Fig. 7(c)]. This causes significant variations in the inter-pillar plasmon coupling and affects the uniformity of the electromagnetic hot spots formed by leaning Ag NP structures.[9,10] The SERS signal intensity fluctuation observed for the 4×10^{-5}-M FA concentration is therefore primarily due to variations in the Ag NP cluster size that produces variations in the enhancement factor of the SERS substrate. Therefore, the abrupt intensity increase is probably not related to the changes in the Ag–FA binding mechanism.

Conclusions

The study of the adsorption of FA on Ag NPs is carried out using SERS spectroscopy and DFT calculations. The comparison between SERS and Raman scattering spectra shows that the interaction of the FA with the nanostructured silver surface is mainly through the nitrogen of the pt ring. This feature was further confirmed by the calculation of the optimized geometry of FA adsorbed to a cluster of ten silver atoms. In addition, we demonstrate that FA molecules adsorbed on Ag NPs follow a positive cooperative binding mechanism, from which the adsorption constant and the *n*-index were calculated, being $2.4\times10^{-6}M^{-1}$ and 1.53, respectively. The presented study is an explorative step towards the fabrication of a detection system that is capable of sensing FA or cancer cells over-expressing folate receptors.

Acknowledgements

We are grateful for the financial support provided by H.C. Ørsted Postdoc Stipend and The Danish Concil for Independent Research´s NAnoPLAsmonic Sensors (NAPLAS) Sapere Aude project.

References

[1] M. Harper, K. McKeating, K. Faulds, *Phys. Chem. Chem. Phys.* **2013**, *15*, 5312.
[2] P. Howes, S. Rana, M. Stevens, *Chem. Soc. Rev.* **2014**, *43*, 3835.
[3] G. McNay, D. Eustace, W. Smith, K. Faulds, D. Graham, *Appl. Spectrosc.* **2011**, *65*, 825.
[4] M. Sonntag, J. Klingsporn, A. Zrimsek, B. Sharma, L. Ruvuna, R. Van Duyne, *Chem. Soc. Rev.* **2014**, *43*, 1230.
[5] M. Muniz-Miranda, B. Pergolese, F. Muniz-Miranda, S. Caporali, *J. Alloys Compd.* **2014**, *615*, S357.
[6] Q. Wu, C. Luo, H. Yu, G. Kong, J. Hu, *Chem. Phys. Lett.* **2014**, *608*, 35.
[7] R. Jarvis, H. Johnson, E. Olembe, A. PAnneerselvam, M. Malik, M. Afzaal, P. O´Brien, R. Goodacre, *Analyst* **2008**, *133*, 1449.
[8] B. Sharma, M. Cardinal, S. Kleinman, N. Greeneltch, R. Frontiera, M. Blaber, G. Schatz, R. Van Duyne, *MRS BULLETIN* **2013**, *38*, 615.

[9] M. S. Schmidt, J. Hübner, A. Boisen, *Adv. Mater.* **2012**, *24*, 11.
[10] K. Wu, T. Rindzevicius, M. S. Schmidt, K. Mogensen, A. Hakonen, A. Boisen, *J. Phys. Chem. C* **2015**, *119*, 2053.
[11] J. Yang, M. Palla, F. Bosco, T. Rindzevicius, T. Alstrøm, M. S. Schmidt, A. Boisen, J. Ju, Q. Lin, *ACS Nano* **2013**, *7*, 5350.
[12] M. Hu, F. Suong, W. Wu, I. Naumov, X. Li, A. Bratkovsky, R. Williams, Z. Li, *J. Am. Chem. Soc.* **2010**, *132*, 12820.
[13] F. Suong, M. Hu, I. Naumov, A. Kim, W. Wu, X. Li, A. Bratkovsky, X. Li, R. Williams, Z. Li, *Nano Lett.* **2011**, *11*, 2538.
[14] A. Kim, F. Suong, D. Ohlberg, M. Hu, R. Williams Z. Li, *J. Am. Chem. Soc.* **2011**, *133*, 8234.
[15] T. Kokaislová, M. Helešicova, M. Ončak, P. Matějka, *J. Raman Spectrosc.* **2014**, *45*, 750.
[16] Y. Qi, Y. Hu, M. Xie, D. Xing, H. Gu, *J. Raman Spectrosc.* **2011**, *42*, 1287.
[17] M. Pagliai, S. Caporali, M. Muniz-miranda, G. Pratesi, V. Schettino, *J. Phys. Chem. Lett.* **2012**, *3*, 242.
[18] L. Zhang, Y. Fang, P. Zhang, *Chem. Phys. Lett.* **2008**, *451*, 102.
[19] R. Stokes, E. McBride, C. Wilson, J. Girkin, E. Smith, D. Graham, *Appl. Spectrosc.* **2008**, *62*, 371.
[20] A. Kokaislová, P. Matějka, *Anal. Bioanal. Chem.* **2012**, *403*, 985.
[21] C. Jing, Y. Fang, *Chem. Phys.* **2007**, *332*, 27.
[22] R. Liu, D. Zhang, C. Cai, Y. Xiong, S. Li, Y. Su, M. Si, *Vib. Spectrosc.* **2013**, *67*, 71.
[23] J. Castillo, W. E. Svendsen, N. Rozlosnik, P. Escobar, F. Martínez, J. Castillo-León, *Analyst* **2013**, *138*, 1026.
[24] X. Wang, T. Zhang, X. Zhao, Z. Guan, Z. Wang, Z. Zhu, Q. Xie, J. Wang, B. Niu, *J. Chromatogr. B* **2014**, *962*, 9.
[25] E. De Bruyn, B. Gulbis, F. Cotton, *Eur. J. Haematol.* **2014**, *92*, 354.
[26] J. Castillo, T. Rindzevicius, K. Wu, M. S. Schmidt, K. A. Janik, A. Boisen, W. Svendsen, N. Rozlosnik, J. Castillo-León, *J. Nanopart. Res.* **2014**, *16*, 2525.
[27] J. J. Castillo, T. Rindzevicius, L. V. Novoa, W. E. Svendsen, N. Rozlosnik, A. Boisen, P. Escobar, F. Martínez, J. Castillo-León, *J. Mater. Chem. B.* **2014**, *1*, 1475.
[28] S. Boca-Farcau, M. Potara, T. Simon, A. Juhem, P. Baldeck, S. Astilean, *Mol. Pharmaceutics* **2011**, *11*, 391.
[29] C. Hu, Y. Liu, J. Qin, G. Nie, B. Lei, Y. Xiao, M. Zheng, J. Rong, *ACS Appl. Mater. Interfaces* **2013**, *5*, 4760.
[30] W. Ren, Y. Fang, E. Wang, *ACS Nano* **2011**, *5*, 6425.
[31] K. Sakata, K. Tada, S. Yamada, Y. Kitagawa, T. Kawakami, S. Yamanaka, M. Okumur, *Mol. Phys.* **2013**, *112*, 385.
[32] P. J. Hay, W. R. Wadt, *J. Chem. Phys.* **1985**, *82*, 270.
[33] P. J. Hay, W. R. Wadt, *J. Chem. Phys.* **1985**, *82*, 299.
[34] R. G. Pearson, *Proc. Natl. Acad. Sci.* **1986**, *83*, 8440.
[35] S. Ana, P. Corio, S. Costa, A. Ando, *Phys. Chem. Chem. Phys.* **2012**, *14*, 15645.
[36] J. Castillo, C. E. Rozo, J. Castillo-León, T. Rindzevicius, W. E. Svendsen, N. Rozlosnik, A. Boisen, F. Martínez, *Chem. Phys. Lett.* **2013**, *564*, 60.
[37] L. Angeles, *FASEB* **1977**, *11*, 835.
[38] S. Thomas, N. Biswas, V. V. Malkar, T. Mukherjee, S. Kapoor, *Chem. Phys. Lett.* **2010**, *491*, 59.

Supporting information

Additional supporting information may be found in the online version of this article at the publisher's website.